AFOSR-TN-59-1101

CALIFORNIA INSTITUTE OF TECHNOLOGY

Antenna Laboratory

Technical Report No. 22

RADIATION PATTERNS OF THE NOISE EMISSION FROM A GASEOUS DISCHARGE

Nick George

This research was supported by the U. S. Air Force through the Air Force Office of Scientific Research of the Air Research and Development Command, under Contract No. AF18(600)-1113. Reproduction in whole or in part is permitted for any purpose of the United States Government.

CONTENTS

ABSTRACT 1

1. INTRODUCTION 2

2. THEORETICAL RADIATION PATTERNS 3

   2.1 Approximate Aperture Illumination for the Thin Slot 5

   2.2 Radiation in the Fraunhofer Region 9

   2.3 Radiation Pattern for the Delta-Correlated Source 11

   2.4 Selected Cases 14

3. EXPERIMENTAL RADIATION PATTERNS 16

   3.1 Description of the Measurement 17

   3.2 Measurements 20

   3.3 Comparison to the Theory 24

4. CONCLUSIONS 26

5. ACKNOWLEDGEMENT 27

REFERENCES 28

FIGURES

1. Coordinates for the Thin Slot

2. Induced Current Approximation

3. Transmission-Line Model for the Aperture Distribution of the Electric Field

4. Thermal Radiation Patterns for Thin Slots of Various Lengths

5. Thermal Radiation Patterns with Lossy Propagation along the Slot

6. Thermal Radiation Pattern for a Thin Slot of 7.3π radians in Length. Data are Taken for $r_o = 1.500$ m, f = 9200 mc/s, and $\Omega = 2.7 \times 10^{-3}$ sterad.

7. Thermal Radiation Pattern for a Thin Slot of 9.5π radians in Length. Data are Taken for $r_o = 1.500$ m, f = 9200 mc/s, and $\Omega = 2.7 \times 10^{-3}$ sterad.

8. Radiation Level as a Function of Pressure for Argon. Data are Taken for $r_o = 1.500$ m, f = 9200 mc/s, $\theta = \pi/2$, $\Omega = 2.7 \times 10^{-3}$ sterad, and no Slotted Metallic Plane.

9. Radiation Pattern at Optical Frequencies with the Same Slot as in Figure 7.

RADIATION PATTERNS OF THE NOISE EMISSION FROM A GASEOUS DISCHARGE

Nick George

ABSTRACT

Theoretical and experimental radiation patterns are given in spectral form for the thermal radiation from a cylindrical discharge column which is adjacent to a long thin slot in a metallic plane. A spatial distribution is predicted which exhibits interference minima and maxima when the length of the slot and the wavelength of the emission are the same order of magnitude. The analysis is based on Maxwell's equations and the Leontovich-Rytov distributed-source generalization of Nyquist's noise formula.

Fraunhofer pattern measurements are presented in which an argon source is used to excite slots of 7.3π and 9.5π radians in length. Data are also presented to show the effects of variations in the pressure and the d-c current of the discharge. The pattern measuring apparatus is a Dicke radiometer having the following characteristics: frequency 9200 mc/s, bandwidth to the detector 16 mc/s, modulation frequency 1000 c/s, and residual noise level 0.3 rms ^{o}K.

An interference phenomenon is predicted by the theory and demonstrated by an experiment, even though the source excitation is spatially distributed and essentially uncorrelated in time and in space. The patterns are not even approximately Lambertian, e.g., a thin slot of 9.5π radians exhibits a pattern having nine relative maxima in 180^{o} with the maximum emission at 63^{o} from the normal.

Radiation Patterns of the Noise Emission from a Gaseous Discharge

1. Introduction

The chaotic motion of the electrons in a plasma or in a metal gives rise to electromagnetic radiation over a wide spectrum which includes the microwave frequencies. The terminal characteristics of such noise sources have been studied both theoretically[1,2] and experimentally[3,4]. In this paper, attention is directed, however, to a problem in which the distributed character of the noise source is of primary importance; specifically, the problem is to determine the far-zone radiation pattern for a noise-excited slot. In the analysis, it is necessary to use a distributed source description, rather than a terminal one; and for this purpose, the formula derived by Leontovich and Rytov[5] is appropriate. Their expression for the correlation function of the x-component of the effective noise electric field in a conductive medium is given by

$$\langle E_x(\underline{r},t)\ E_x^*(\underline{r}-\underline{r}_o,t-t_o)\rangle = \frac{2\bar{\epsilon}}{\sigma}\,\delta(\underline{r}_o)\,\delta(t_o) \quad . \tag{1}$$

If a generalized Ohm's law holds for the medium, i.e., if $j(r)=\sigma_c E(r)$, then an equivalent expression for the correlation function of the x-component of the current density is given by

$$\langle j_x(\underline{r},t)\ j_x^*(\underline{r}-\underline{r}_o,t-t_o)\rangle = 2\epsilon\sigma\,\delta(\underline{r}_o)\,\delta(t_o) \quad . \tag{2}$$

$E_x(\underline{r},t)$ and $j_x(\underline{r},t)$ are the x-components of the source electric field and the current density, respectively; $\delta(\underline{r})$ is Dirac's delta function; σ is the real part of the complex conductivity σ_c; and $\bar{\epsilon}$ is the mean energy per degree of freedom given by Planck as

$$\bar{\epsilon} = \frac{hf}{e^{hf/kT} - 1} , \tag{3}$$

where f is the frequency, T is the absolute temperature, h is Planck's constant, and k is the Boltzmann constant.

The angular parentheses, $\langle\ \rangle$, are used throughout this paper to denote an ensemble average. A second notational convenience, adopted herein, is that time dependence is always indicated explicitly while frequency dependence is not. Therefore, $E(x,y)$ may mean $E(x,y,\omega)$, but it will never mean $E(x,y,t)$.

An important result in spectral analysis is quoted for later use. Let $f(x,t)$ be a sample function of a stationary random process. It can be shown that the two-dimensional correlation function and the mixed spectral density and correlation function satisfy the following Fourier transform relationship.

$$\int_{-\infty}^{\infty} \langle f(x_1,t)\ f^*(x_2,t-t_o)\rangle\ e^{-i\omega t_o}\, dt_o = \lim_{2T\to\infty} \left\langle \frac{F(x_1,\omega)\ F^*(x_2,\omega)}{2T} \right\rangle \tag{4}$$

in which

$$F(x,\omega) = \int_{-T}^{T} f(x,t) e^{-i\omega t}\, dt \quad .$$

2. Theoretical Radiation Patterns

Consider a metallic plate in the $y = 0$ plane with a long thin z-oriented aperture of dimensions (a,b) where $a \gg b$ (see Fig. 1). The aperture is illuminated or excited by a distributed noise source that generates electromagnetic energy which is incoherent spatially and timewise, e.g., a closely-spaced hot wire or a plasma column. An

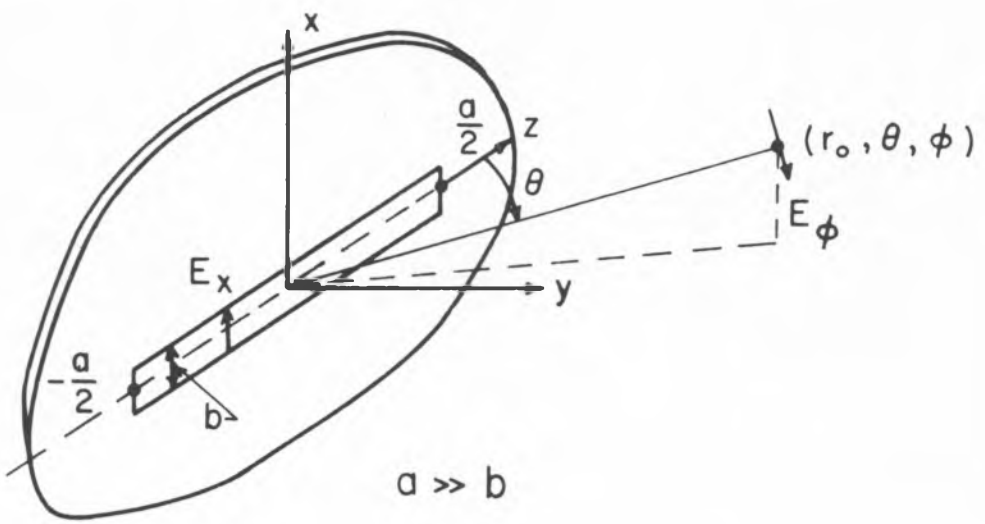

Figure 1. Coordinates for the Thin Slot

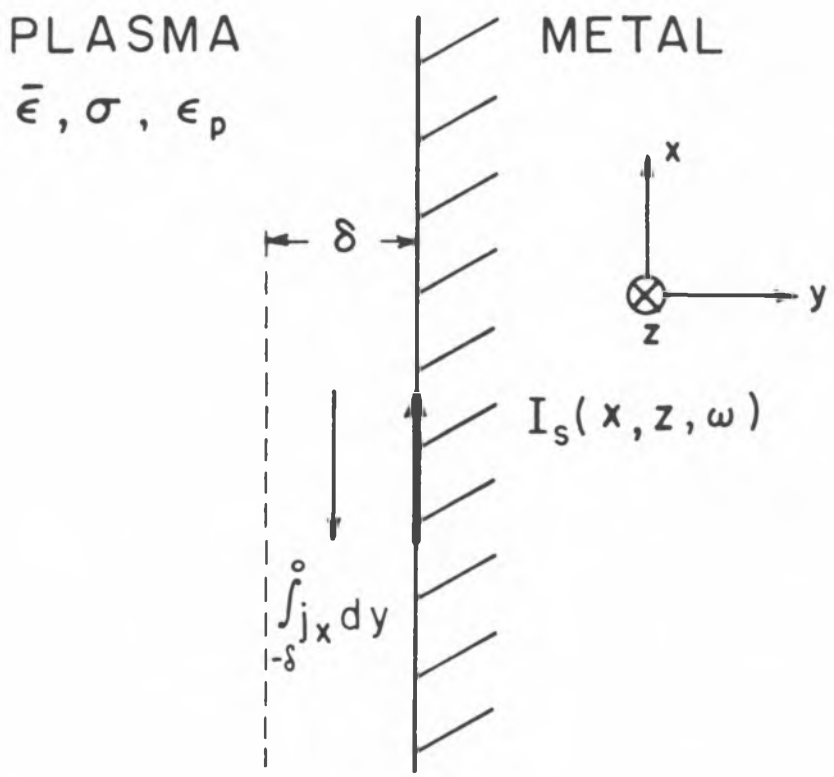

Figure 2. Induced Current Approximation

approximate analysis for the resultant aperture distribution is made in the following section. The effects of radiation losses are neglected; and furthermore, aside from the generation of the noise, the influence of the noise medium of contrasting dielectric constant and conductivity is assumed calculable by allowing for a perturbation in the propagation constant for the region surrounding the slot.

2.1 Approximate Aperture Illumination for the Thin Slot

A source current per unit length, $I_s(x,z,\omega)$, is induced in the metallic plane (see Fig. 2). An approximate value for this current is obtained in the following manner. Let the noise source, rapidly moving plasma electrons, fill the half-space for which $y < 0$, and suppose that the plate at $y = 0$ is not slotted. The moving electrons induce eddy currents; but over the range of frequencies for which the plasma is opaque, only those electrons close to the plate are effective in inducing these currents. It is assumed that the characteristic depth is the absorption skin depth of the plasma, δ. Thus, when averaged over the narrow dimension of the slot, the x-component of the surface current per unit length, $I_s(z,\omega)$, is given by

$$I_s(z,\omega) = \frac{1}{b} \int_{-b/2}^{b/2} I_s(x,z,\omega)\, dx$$

or, in terms of j_x, by

$$I_s(z,\omega) = \frac{1}{b} \int_{-\delta}^{0} \int_{-b/2}^{b/2} j_x(x,y,z,\omega)\, dx\, dy \quad , \tag{5}$$

where the integrations are required in order to take account of the

spatial incoherence of the noise currents. Equations (2),(4),(5) are combined to give the following mixed spectral density and correlation function for the x-component of the source current in the metal plate.

$$\lim_{2T\to\infty} \left\langle \frac{I_s(z_1,\omega)\, I_s^*(z_2,\omega)}{2T} \right\rangle = \frac{2\bar{\epsilon}\,\sigma\,\delta}{b}\,\delta(z_1-z_2) \quad . \tag{6}$$

Now with a slotted plane, the influence of the source current, I_s, in the region from z to $z + dz$ is felt everywhere along the gap. Consider the principal mode analysis in which the slot is viewed as a transmission line with the source field propagating mainly along the gap and with a standing wave being established by the reflections at $z = \pm a/2$ (see Fig. 3). The transmission line equations are

$$\frac{\partial V}{\partial z} = - Z'I \tag{7}$$

and

$$\frac{\partial I}{\partial z} = - Y'V + I_s \ , \tag{8}$$

where the series impedance per unit length, Z', and the shunt admittance per unit length, Y', are related to the complex propagation factor, $\beta_c = \beta - i\alpha$, by

$$\beta_c^2 = - Y'Z' \tag{9}$$

and where the potential, V , is defined by $V = \int_{-b/2}^{b/2} E_x(x,0,z,\omega)dx$.

Taking $\partial/\partial z$ of eq. (7) and substituting from eqs. (8),(9) give the wave equation for V ,

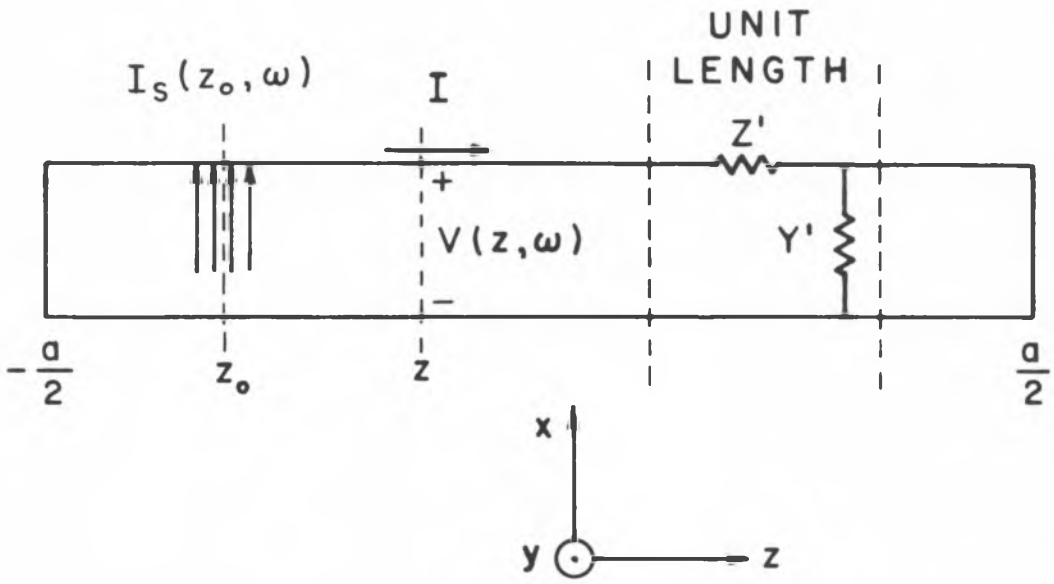

Figure 3. Transmission-Line Model for the Aperture Distribution of the Electric Field

$$\frac{\partial^2 V}{\partial z^2} + \beta_c^2 V = - Z' I_s \quad . \tag{10}$$

The general solution of eq. (10), subject to the boundary condition that $V(\pm a/2,\omega) = 0$, is readily obtained by standard methods; and the result is given by

$$V(z,\omega) = \int_{-a/2}^{+a/2} Z' I_s(z_o,\omega) \frac{1}{2\beta_c} \left[\frac{\cos \beta_c(z+z_o) - \cos \beta_c(a-|z-z_o|)}{\sin \beta_c a} \right] dz_o \tag{11}$$

where an alternative special form must be written for the cases in which $\beta_c a = \pi, 2\pi, 3\pi, \cdots$.

In the final result, an expression containing Z' is not convenient. This series impedance per unit length can be eliminated in favor of a more fundamental impedance parameter by means of an approximate relation developed in eq. (14) below. Using the form of Babinet's principle as generalized for vector fields by Booker[6,7], one can readily establish the following relationship between Z',Y' for a slot and the corresponding Z'',Y'' for the complementary electric dipole, i.e., a thin metallic strip of cross-section a by b .

$$\frac{Z'}{Y''} = \frac{\eta^2}{2} \qquad \text{and} \qquad \frac{Y'}{Z''} = \frac{2}{\eta^2} \quad . \tag{12}$$

Then, using the transmission line model for the metallic dipole and expressing the input impedance of a center-driven antenna in terms of an open-circuited line of length $a/2$, one obtains

$$Y'' = \frac{\beta_c \cot \frac{\beta_c a}{2}}{z_{in}} \quad , \tag{13}$$

in which z_{in} is the input impedance of the center-driven metallic dipole of length a. Strictly, the admittance per unit length varies along the length of the antenna; hence, eq. (13) should be regarded as a defining equation for an averaged admittance to be used with the transmission line model*. Combining eqs. (12),(13) one obtains the final expression for the Z' of the slot, i.e.,

$$Z' = \frac{\eta^2 \beta_c \cot \frac{\beta_c a}{2}}{2z_{in}} \quad . \tag{14}$$

Elimination of Z' in eq. (11) by eq. (14) gives the following result for the aperture illumination:

$$V(z,\omega) = \frac{\eta^2}{4z_{in}} \int_{-a/2}^{a/2} I_s(z_o,\omega) \left[\frac{\cos \beta_c(z+z_o) - \cos \beta_c(a - |z-z_o|)}{1 - \cos \beta_c a} \right] dz_o \, . \tag{15}$$

2.2 Radiation in the Fraunhofer Region

The approximate tangential electric field over the $y = 0$ plane is now determined. The specification of the tangential electric field over this plane together with the radiation condition for the field as $r_o \to \infty$ are sufficient to uniquely determine the radiation field. The radiation field is conveniently expressed in terms of the Fourier integral analogue of eq. (1-14.19) of Smythe[9]. This formula gives the exact diffracted vector potential in terms of the aperture

*The result in eq. (13) can also be deduced in another, perhaps more fundamental, way from eqs. (19),(24),(25) of Weber[8].

distribution for an arbitrary aperture. Differentiating, since $E = -\partial A/\partial t$, suppressing the $e^{i\omega t}$ factor, dropping the near-zone term, and making the usual far-zone approximation in the phase term, i.e., $r \approx r_o - z_1 \cos\theta$, one can reduce eq. (1-14.19) to the following form:

$$E_\phi(r_o,\theta,\phi,\omega) = \frac{-i\beta_o \sin\theta\, e^{-i\beta_o r_o}}{2\pi r_o} \int_{-a/2}^{a/2} V(z,\omega)\, e^{i\beta_o z\cos\theta}\, dz \qquad (16)$$

in which the coordinates (r_o,θ,ϕ) are shown in Fig. 1.

In the far-zone, the power radiated through a solid angle $d\Omega$ is given by Poynting's theorem as the product $[r_o E_\phi(r_o,\theta,\phi,t)]^2 d\Omega/\eta$. From this, it follows that in spectral form, the average power radiated through a solid angle $d\Omega$ in the frequency interval df is given by

$$P_{f\Omega}\,df\,d\Omega = \lim_{2T\to\infty} \frac{2r_o^2}{\eta} \left\langle \frac{E_\phi(r_o,\theta,\phi,\omega)\, E_\phi^*(r_o,\theta,\phi,\omega)}{2T} \right\rangle df\,d\Omega \ . \qquad (17)$$

Arbitrarily, the power through a unit solid angle per unit frequency interval, $P_{f\Omega}$, is defined above on the basis of a one-sided frequency interval, i.e., the total average power per solid angle is given by $\int_0^\infty P_{f\Omega}\,df$. Substitution of eqs. (15),(16) into eq. (17) gives the following integral form for the radiation pattern of the slot:

$$P_{f\Omega} = \frac{\eta}{8\pi^2}\left[\frac{\eta\,|\beta_c|\sin\theta}{|z_{in}|\,\beta_o}\right]^2 \int_{-\frac{a}{2}}^{\frac{a}{2}}\int_{-\frac{a}{2}}^{\frac{a}{2}}\int_{-\frac{a}{2}}^{\frac{a}{2}}\int_{-\frac{a}{2}}^{\frac{a}{2}} \lim_{T\to\infty}\left\langle\frac{I_s(z_o,\omega)I_s^*(z_1,\omega)}{2T}\right\rangle$$

$$\times\left[\frac{\cos\beta_c(z_2+z_o)-\cos\beta_c(a-|z_2-z_o|)}{2\beta_c(1-\cos\beta_c a)}\right]\left[\frac{\cos\beta_c(z_3+z_1)-\cos\beta_c(a-|z_3-z_1|)}{2\beta_c(1-\cos\beta_c a)}\right]^*$$

$$\times e^{i\beta_o(z_2-z_3)\cos\theta}\,\beta_o^4\,dz_o\,dz_1\,dz_2\,dz_3 \quad . \tag{18}$$

2.3 Radiation Pattern for the Delta-Correlated Source

Equation (18) is integrated directly with respect to the variables z_2 and z_3. Then, eq. (6) is substituted for the source function, and the expression is integrated with respect to z_o and z_1. These integrations lead in a tedious but straightforward way to the intermediate form given below.

$$P_{f\Omega} = \frac{\eta\bar{\epsilon}\sigma\delta}{4\pi^2 b}\left[\frac{\eta|\beta_c|}{|z_{in}|\beta_o}\right]^2 \frac{4\beta_o^4\sin^2\theta}{\left|1-\cos\beta_c a\right|^2\left|\beta_c^2-(\beta_o\cos\theta)^2\right|^2}\,K_1 \quad , \tag{19}$$

in which

$$K_1 = a\left|\sin\beta_c\frac{a}{2}\cos\beta_c\frac{a}{2}\right|^2 +$$

$$+\frac{\sinh\alpha a}{2\alpha}\left[\left|\sin\beta_c\frac{a}{2}\right|^2\cos^2\left(\beta_o\frac{a}{2}\cos\theta\right)+\left|\cos\beta_c\frac{a}{2}\right|^2\sin^2\left(\beta_o\frac{a}{2}\cos\theta\right)\right]$$

$$+\frac{\sin\beta a}{2\beta}\left[\left|\sin\beta_c\frac{a}{2}\right|^2\cos^2\left(\beta_o\frac{a}{2}\cos\theta\right)-\left|\cos\beta_c\frac{a}{2}\right|^2\sin^2\left(\beta_o\frac{a}{2}\cos\theta\right)\right]$$

$$+\mathrm{Re}\,\frac{\beta_c^*\sin\beta_c a}{\beta_c^{*2}-(\beta_o\cos\theta)^2}\left[\cos\beta_c^* a-\cos(\beta_o a\cos\theta)\right] \quad .$$

Equation (19) is not in a convenient form for computation. A more

convenient form is obtained by introducing a $(4\beta_o)$ portion of the coefficient into the central bracket, replacing β_o/η by $\omega\epsilon_o$, and eliminating β_c in favor of α,β. Finally, after considerable manipulation, the following expression is obtained for the one-sided spectral intensity of the power which is radiated per unit frequency per unit solid angle:

$$P_{f\Omega} = \frac{\sigma\delta\bar{\epsilon}\,\eta^2\,(\rho^2+\gamma^2)\,\sin^2\theta\;\; K_2}{4\pi^2\omega\epsilon_o b|z_{in}|^2[\cosh\alpha a-\cos\beta a]^2[(\gamma^2-\rho^2-\cos^2\theta)^2+4(\gamma\rho)^2]} \qquad (20)$$

in which

$$K_2 = \beta_o a\left\{\frac{\sinh\alpha a}{\alpha a}\left[\cosh\alpha a-\cos(\beta_o a\cos\theta)\cos\beta a\right]+\frac{1}{2}\cosh 2\alpha a-\frac{1}{2}\cos 2\beta a\right\}$$

$$+\frac{\beta_o\sin\beta a}{\beta}\left[-\cos\beta a+\cos(\beta_o a\cos\theta)\cosh\alpha a\right]\;+$$

$$+\frac{4}{(\gamma^2-\rho^2-\cos^2\theta)^2+4(\gamma\rho)^2}\left\{\gamma\left[\gamma^2+\rho^2-\cos^2\theta\right]\sin\beta a\right.$$

$$\times\left[\cos\beta a-\cos(\beta_o a\cos\theta)\cosh\alpha a\right]$$

$$\left.-\rho\left[\gamma^2+\rho^2+\cos^2\theta\right]\sinh\alpha a\left[\cosh\alpha a-\cos(\beta_o a\cos\theta)\cos\beta a\right]\right\}$$

and where

$\sigma\delta$ = conductivity, skin-depth product for the plasma,

$i\beta_c = i\beta+\alpha$,

$\gamma = \beta/\beta_o$,

$\rho = \alpha/\beta_o$,

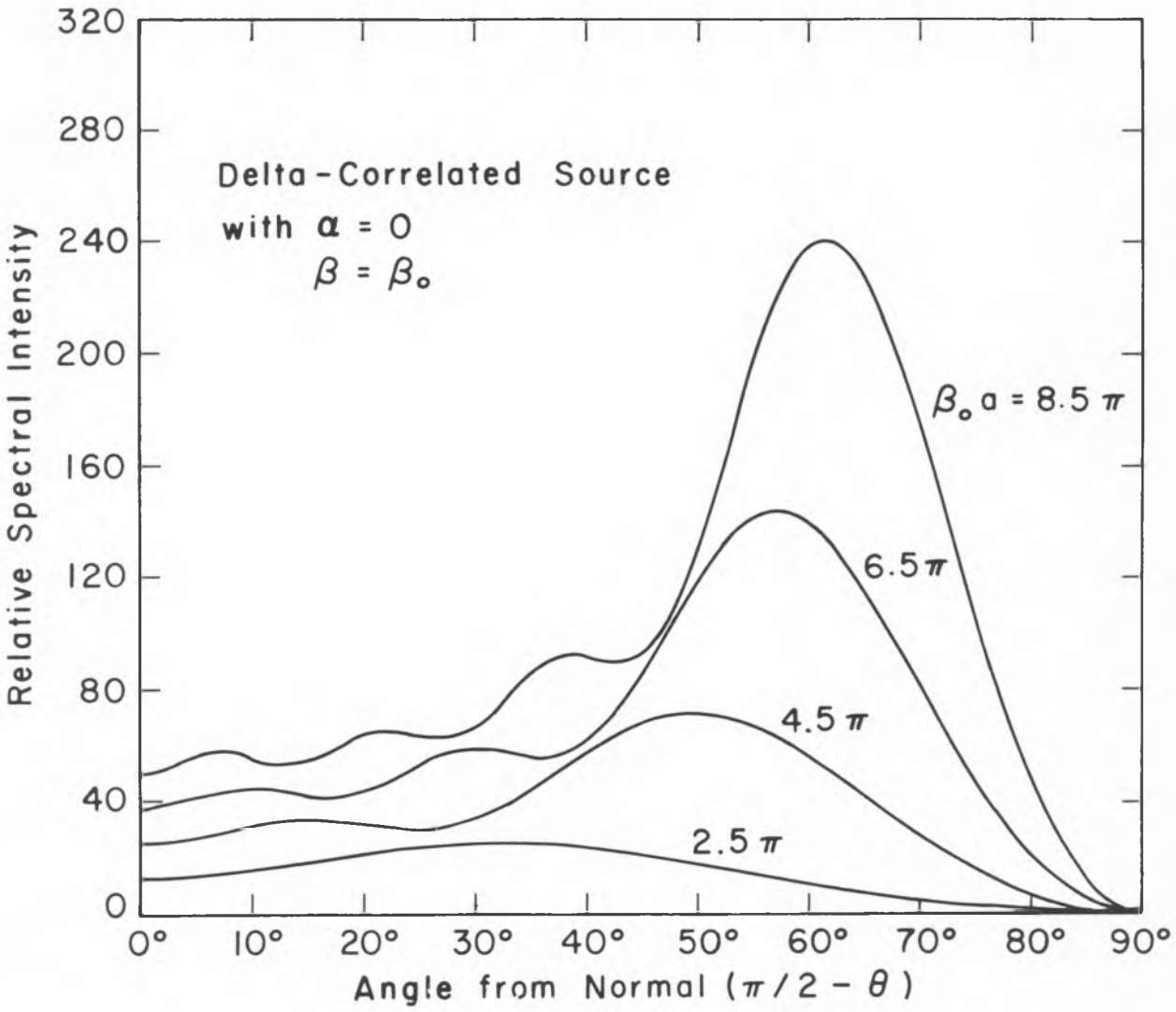

Figure 4. Thermal Radiation Patterns for Thin Slots of Various Lengths

z_{in} = input impedance of center-driven complementary metallic dipole[7],

$\eta = (\mu_o/\epsilon_o)^{1/2}$,

$\omega = 2\pi f$.

The above equation represents a first order approximation to the radiation pattern for a thin slot which is excited incoherently both spatially and timewise. This analysis is similar to that of Levin and Rytov[10] for the thermal radiation pattern of a thin linear antenna. However, even allowing for the complementary aspect, there are two differences. First, the eq. (20) solution appears to apply for a greater range of lengths due to the incorporation of z_{in}.[11] Secondly, a complex wave number is assumed for the propagation along the slot in order to account for loss and phase retardation due to the noise source. Setting $\alpha = 0$ and $\beta = \beta_o$ in eq. (20), one finds that the spatial variation agrees with that obtained by Levin and Rytov.

2.4 Selected Cases

Radiation patterns are plotted for several different slot lengths when there is no loss and when the wave numbers are equal (see Fig. 4). The graphs are of $P_{f\cap}$ (from eq. (20) with $\alpha = 0$, $\beta = \beta_o$) normalized to $\sigma\delta\bar{\epsilon}\eta^2/(4\pi^2\omega\epsilon_o b|z_{in}|^2)$ and plotted versus the angle from the normal, $\pi/2 - \theta$, for values of the length $\beta a/\pi = 2.5$, 4.5, 6.5, and 8.5 .

Radiation patterns are also plotted for a variable loss factor but with a fixed length and with no phase retardation (see Fig. 5). The graphs are of $P_{f\cap}$ (from eq.(20) with $\beta = \beta_o$, $\beta_o a = 9.5\pi$) normalized to $\sigma\delta\bar{\epsilon}\eta^2/(4\pi^2\omega\epsilon_o b|z_{in}|^2)$ and with the attenuation parameter, α , selected to give 0, 1, 3, 5, and 20 decibels of

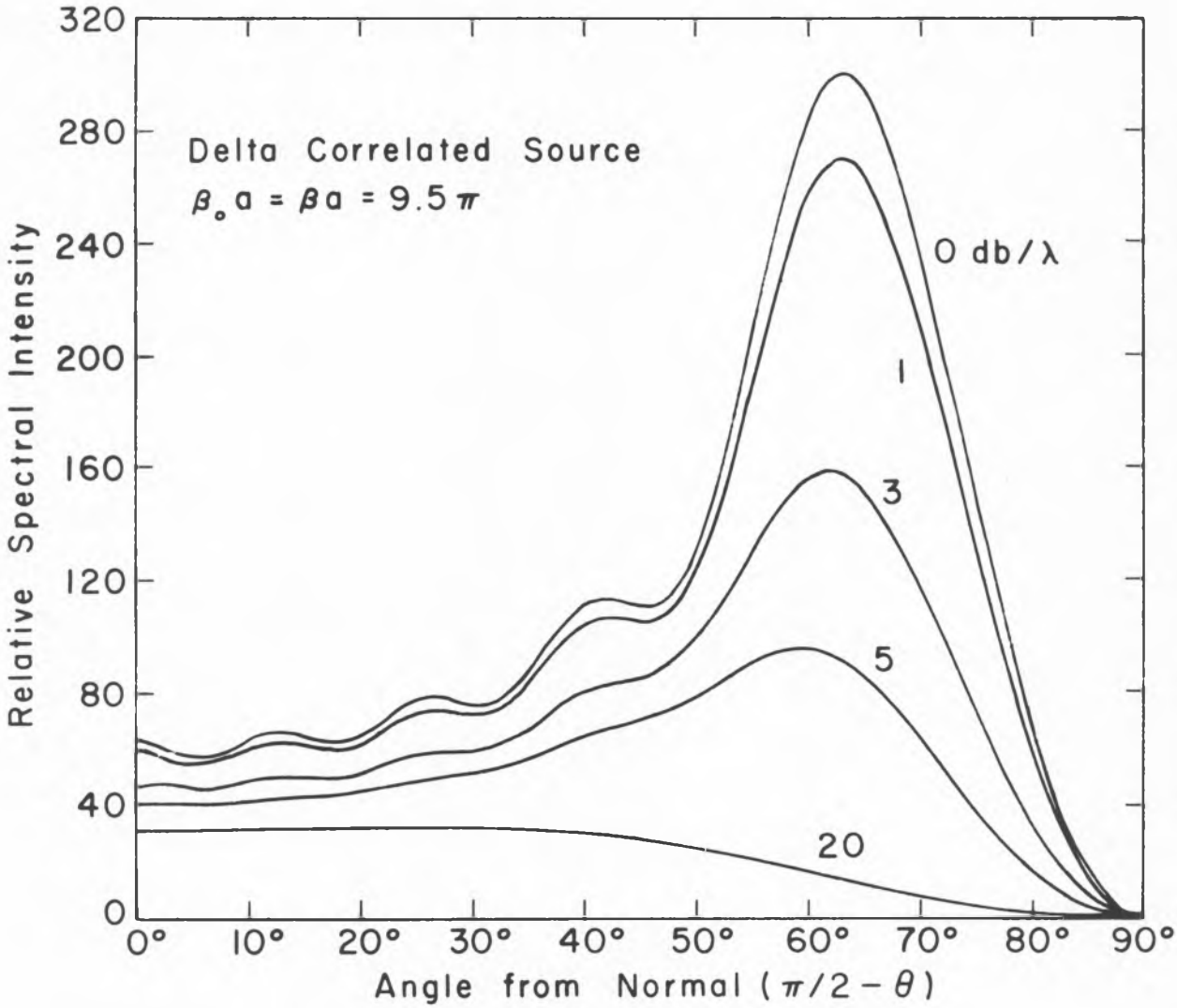

Figure 5. Thermal Radiation Patterns with Lossy Propagation along the Slot

attenuation per wavelength.

3. Experimental Radiation Patterns

There are two radiation experiments which would be very interesting to perform in the course of verifying the theory. One of these is the measurement of the thermal radiation from a hot wire of moderately high conductivity. In order to make this measurement in the far zone at microwave frequencies, it has been estimated that receiver sensitivities of $2\times10^{-3}\,^{\circ}K$ and $0.1\,^{\circ}K$ are required using sources of tungsten and silicon carbide, respectively[11]. Restricting the receiver bandwidth to approximately 100 mc/s in order to prevent excessive smoothing of the pattern, one concludes that with the best present-day receiver this measurement is practical using silicon carbide or a similar material, but not using tungsten. However, near-zone measurements of the microwave radiation from incandescent tungsten are practical; and in fact, such a measurement has been described by Westberg[12]. A theoretical analysis of the near-zone case has not appeared in the literature.

The other experiment of interest is the measurement of the thermal radiation from a noise-excited thin slot. For this latter experiment, using a gaseous discharge as a source, one finds, as detailed below, that a receiver sensitivity of $1\,^{\circ}K$ or $2\,^{\circ}K$ is sufficient to permit pattern measurements in the far-zone. This sensitivity is considerably less than is quoted above for the experiments using a hot-wire source. This is due both to the much higher radiation temperature and to the higher emissivity of the gaseous discharge source.

3.1 Description of the Measurement

From a conceptual point of view, the measurement of a radiation pattern is quite simple. Briefly, a receiver and a transmitter are positioned at some fixed separation. For either antenna, the radiation pattern is simply the received signal as a function of the angular position as the antenna being measured is rotated about its center.

In these experiments, the transmitting antenna is typically a 4.75 by 0.122 wavelength slot in a 28 by 19 wavelength metallic ground plane. The source of the thermal radiation is an argon glow discharge tube* clamped to the ground plane and running along the length of the slot. This entire ground plane assembly is mounted on a wooden turntable with provisions for measuring the angle of rotation.

The receiving aperture is a microwave horn which is positioned at a 1.500 m range with the electric-field polarization perpendicular to the long edge of the radiating slot, i.e., placed at $(1.500, \theta, \pi/2)$ to read $E_{\phi}(\theta)$ in Fig. 1. The E- and H-plane dimensions of this

---

*The dimensions of the tube are 0.765 cm ID, 0.953 cm OD, and 21.2 cm long. The tube is filled with pure argon; and for these experiments, unless otherwise specified, a pressure of 30.0 ± 0.3 mm Hg and an operating point of 200 ma and 71 v are used. For these values, the kinetic temperature of the plasma electrons is computed from eq.(8.36) of von Engel[13], and the result is a temperature

$$T = 11{,}300^{\circ}\ \mathrm{K}\ .$$

The measured value of the microwave noise temperature is, as expected[2,4], essentially the same, i.e.,

$$T = 10{,}072 \pm 200^{\circ}\ \mathrm{K}\ .$$

aperture are 8.04 cm and 11.10 cm, respectively; and at 9,200 mc/s the measured absolute gain is 72 (versus a theoretical value of 70). Hence, the effective solid angle, computed from $\Omega = G\lambda^2/(4\pi r_o^2)$, is 2.70×10^{-3} sterad. Approximate criteria for the Fraunhofer region require that $r_o > 2a\ell/\lambda$ and $r_o > a^2/\lambda$, in which ℓ is the H-plane dimension of the receiving aperture.[14] For $\beta_o a = 9.5\pi$ and a frequency of 9,200 mc/s, these give $r_o > 1.05$ m and 0.74 m, respectively. Therefore, one concludes that with a slot length of 9.5π radians, a range of 1.500 m places the receiving aperture in the far-zone region.

The problem of detecting the thermal radiation from either a heated wire or a noise-excited thin slot is the same detection problem which is encountered in radio astronomy. In these two applications both the signal and the internal receiver noise have essentially the same wide spectral density. Dicke devised a practical method for detecting such signals, even though they are less than 1/1000th of the level of the receiver noise[15]. A receiver of this basic type was designed for the experiments which are described in this paper. The characteristics of this receiver are briefly summarized as follows: a total fluctuation, drift, and reflection error of 0.3 rms ^oK; an amplification bandwidth of 16 mc/s centered at 9,200 mc/s (9,166 to 9,174 mc/s and 9,226 to 9,234 mc/s); a noise ratio for the mixer and the i-f amplifier of 5(7 db); a modulation frequency of 1,000 c/s; and an integration time of 30 sec. This receiver is calibrated by using an argon noise source and a variable attenuator as a secondary standard. Although these measurements are reproducible to better than 3%, their absolute accuracy is probably no better than 20%.

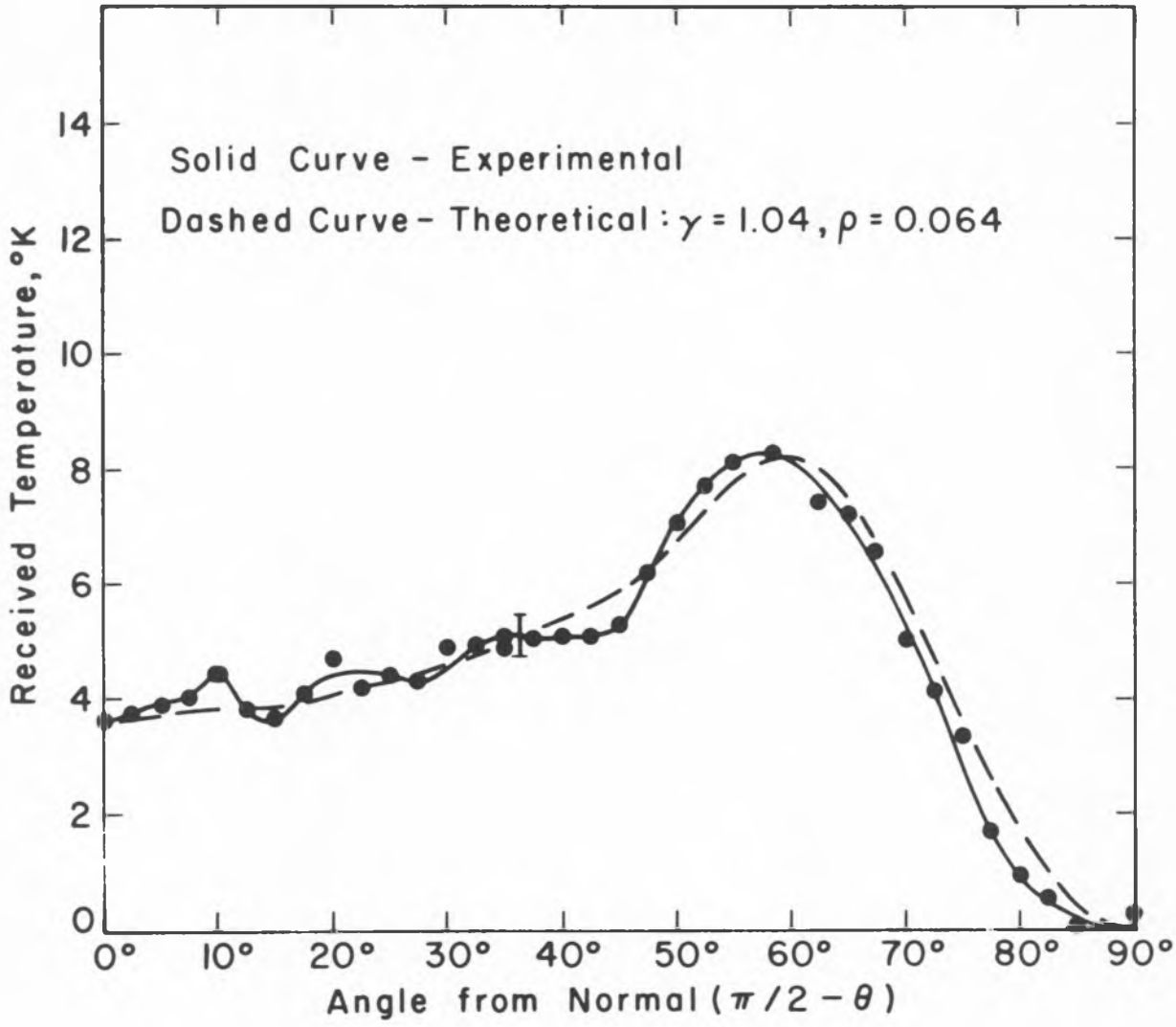

Figure 6. Thermal Radiation Pattern for a Thin Slot of 7.3π Radians in Length. Data are taken for r_o = 1.500m, f = 9,200 mc/s, and $\Omega = 2.7 \times 10^{-3}$ sterad.

3.2 Measurements

Experimental thermal radiation patterns are shown for slot lengths of $\beta_o a = 7.30\pi$ and 9.50π and for a common slot width of $\beta_o b = 0.244\pi$ (see Figs. 6,7). The radiation received from the noise-excited thin slot is expressed in terms of an effective received temperature and this is plotted versus the angle from the normal, $\pi/2 - \theta$. In the notation of Sec. 2, the received temperature is given by solving $kT_a df = P_{f\int\Omega} d\Omega df$ for T_a, i.e., $T_a = P_{f\int\Omega} d\Omega/k$. Only one quadrant of the pattern is plotted due to the symmetry about the plane $\theta = \pi/2$.

In addition, the thermal radiation is measured for several argon-filled tubes at different pressures (see Fig. 8). In this measurement there is no ground plane; but the receiver, the range, and the tube envelope are unchanged. Only the received temperature which is due to the ϕ-component of the noise electric field is shown. However, in the absence of the ground plane, there is also a θ-component of the electric field with a Poynting's vector at $\theta = \pi/2$ of approximately one-half the value of that shown.

In order to permit a comparison of the classical radiation pattern to those above, an experimental curve is also shown for the radiation pattern of the thin slot at optical frequencies (see Fig. 9). Essentially the same experimental arrangement is preserved, except that now a sensitive photocell receiver is used to measure the intensity. The thin slot is of the order of 10^6 wavelengths long at the peak of the spectral response of the photocell.

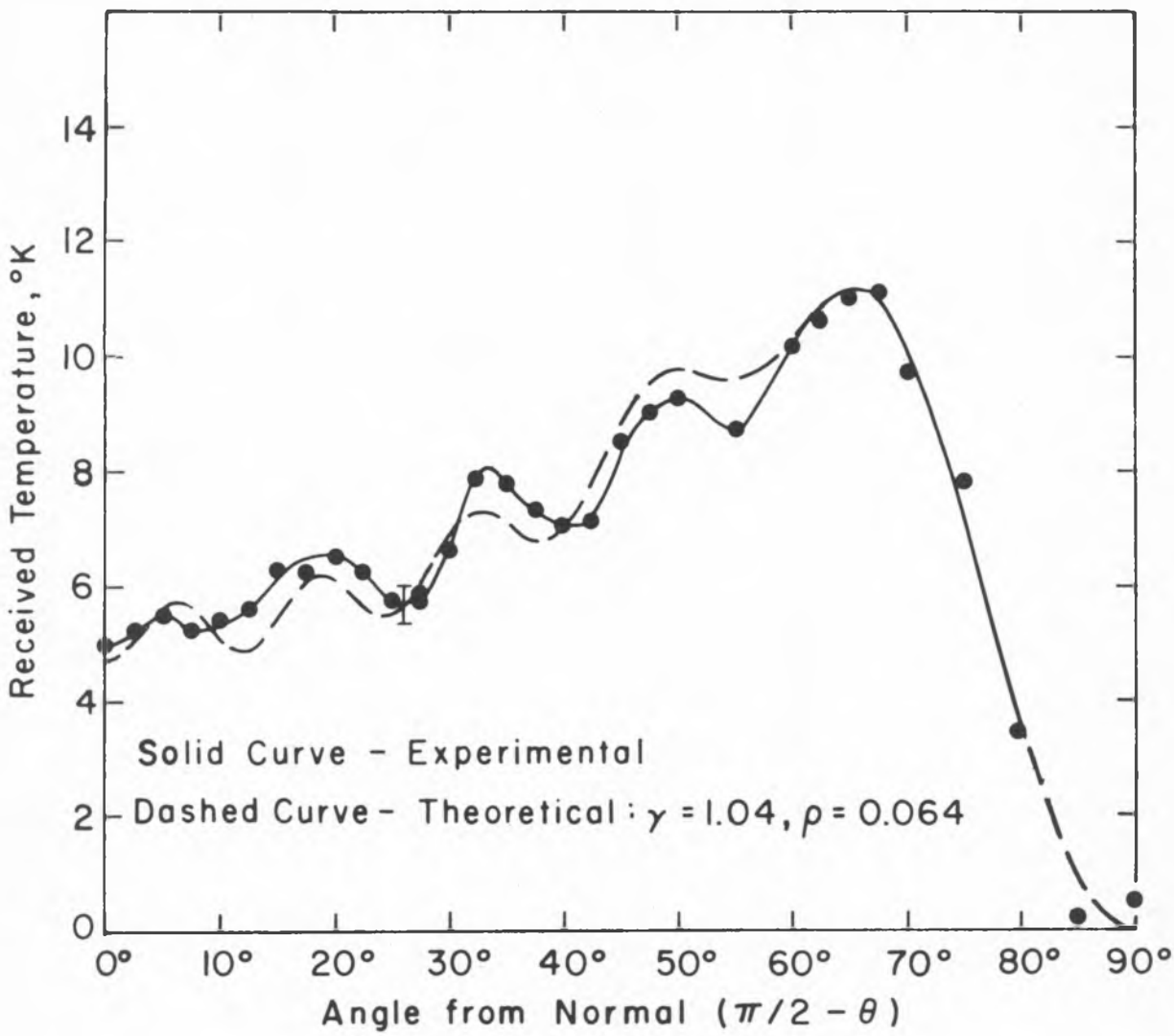

Figure 7. Thermal Radiation Pattern for a Thin Slot of 9.5π Radians in Length. Data are Taken for $r_o = 1.500$m, f = 9,200 mc/s, and $\Omega = 2.7 \times 10^{-3}$ Sterad.

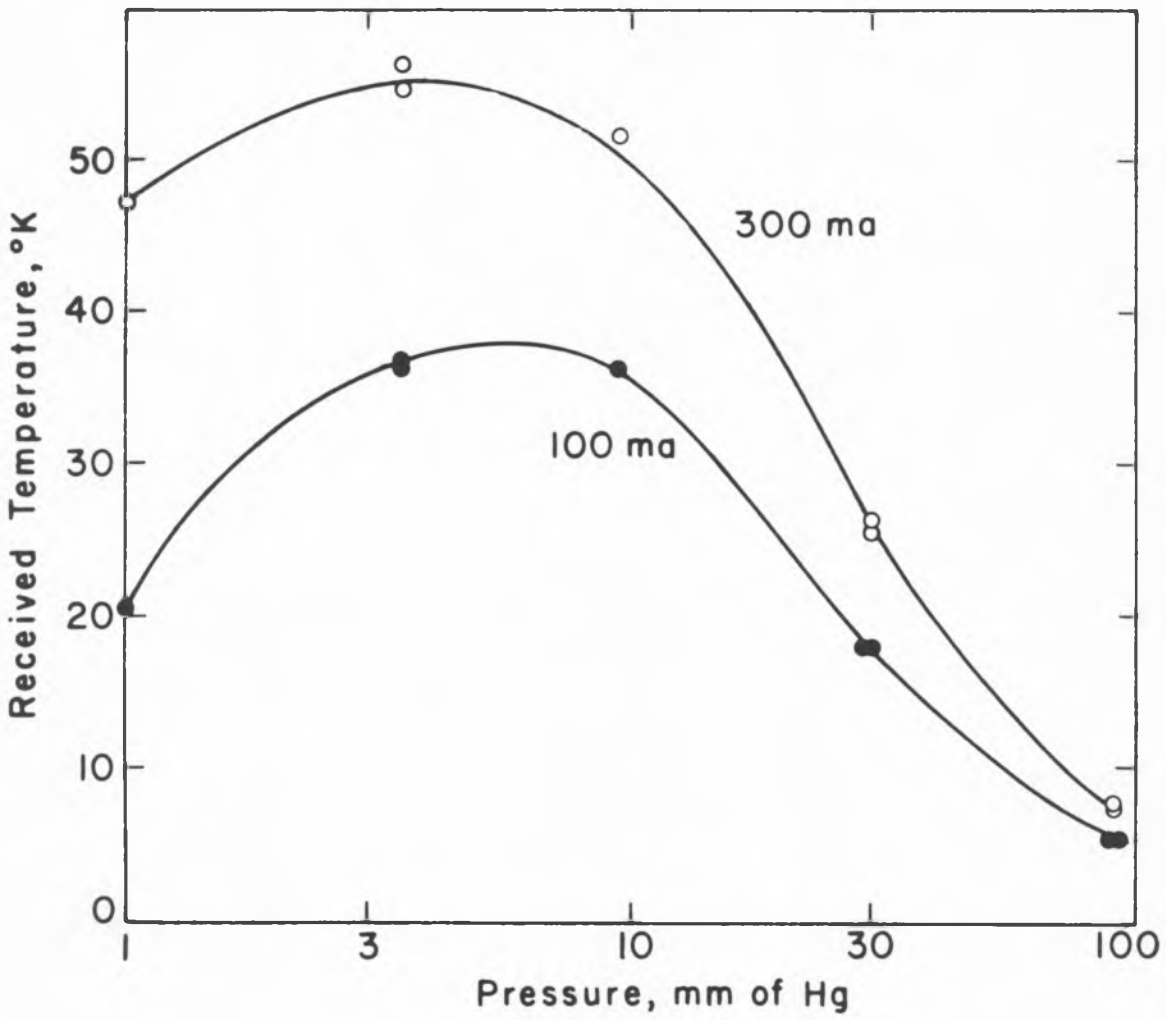

Figure 8. Radiation Level as a Function of Pressure for Argon. Data are Taken for r_o = 1.500m, f = 9,200 mc/s, $\theta = \pi/2$, $\Omega = 2.7 \times 10^{-3}$ Sterad, and no Slotted Metallic Plane.

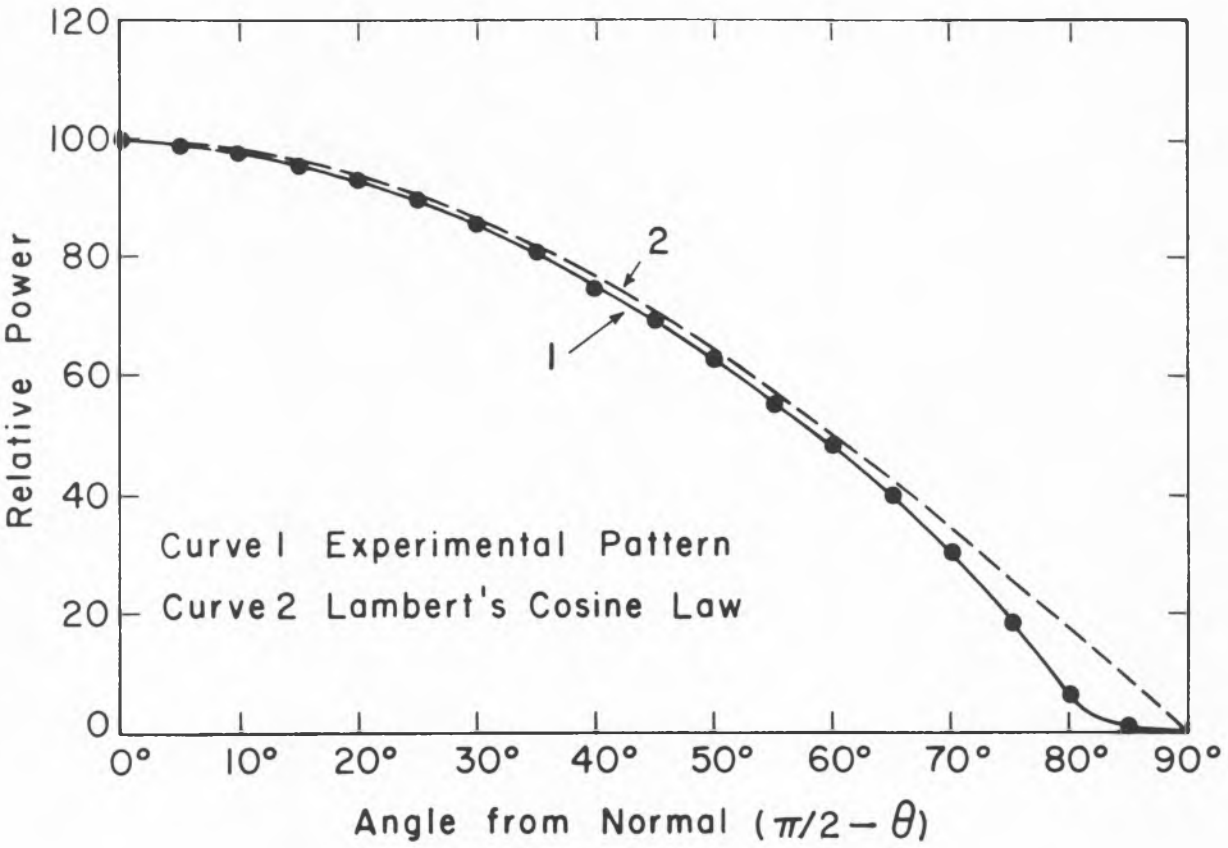

Figure 9. Radiation Pattern at Optical Frequencies with the Same Slot as in Figure 7.

3.3 Comparison to the Theory

First, it is seen that the optical radiation pattern is approximately Lambertian, while the microwave pattern is not. Furthermore, the general features of the microwave pattern measurements agree quite well with the theory which is presented in this paper.

In making a quantitative comparison, it is noted from a computation of eq. (20) for the $\beta = \beta_o$ case, that there are 7 and 9 relative maxima predicted for slots of 7.3π and 9.5π radians in length, respectively. However, from the experimental curves, it is seen that there are 8 and 10 relative maxima observed in these respective cases. Although the geometry makes an exact solution difficult, it is known that the effect of the glass walls of the discharge tube is to decrease the phase velocity along the slot, while that of the plasma column itself is to increase this velocity. Apparently, their combined effect is to slightly decrease the value of the phase velocity from that in free space. Using a phase factor of $\gamma = 1.04$ and an attenuation constant of $\rho = 0.064$ (3.5 db/λ) in eq. (20), one finds fair agreement between the experiment and the theory as is seen by comparing the solid to the dashed curve in Figs. 6,7. The values for γ and ρ have been selected to give a compromise fit for both of the slot lengths. The main discrepancy appears in the $\beta_o a = 7.3\pi$ case, where the observed ripple exceeds the theoretical value. This could be due to the compromise method of selecting γ,ρ or to some more fundamental cause, e.g., a slight degree of coherence in the slot excitation.* The angles at which the

*The radiation patterns for an exponentially-correlated source show the same general features as those given by eq. (20), but the relative ripple is higher even for a correlation length which is less than λ.[11]

relative maxima occur are tabulated (see Tab. 1). In compiling this table, a lower attenuation constant is used for the $\beta_o a = 7.3\pi$ case in order to enhance the ripple and thereby to permit the determination of the tabulated angles.

Tab. 1. Comparison of Experiment to Theory for the Thin Slot

Radian Length ($\beta_o a$)		Angle of Rel. Max. $\lvert \pi/2 - \theta \rvert$	z_{in} (ohms)	T_a at $\theta = \pi/2$ (^oK)
7.3π	Expt.	10,21,36,58	332.	3.6
	Theory	8,26,44,62		$1.89\times10^{4}\sigma\delta$
9.5π	Expt.	5,19,33,50,65	343.	5.0
	Theory	6,19,33,51,65		$2.74\times10^{4}\sigma\delta$

The theoretical curves in Figs. 6,7 are drawn with an arbitrary normalization of the amplitude. Although the precise value of $\sigma\delta$ is not known, it is worthwhile to compare the ratio of the received temperature for the two slots at some convenient angle. Substituting the values $\beta_o a = 7.3\pi$ or 9.5π, $f = 9.2\times10^{9}$ c/s, $b = 3.97\times10^{-3}$ m, $\gamma = 1.04$, $\rho = 0.0641$, and $\theta = \pi/2$, one finds from eq. (20) that $K_2 = 42.92$ or 66.55 and from formulas in Schelkunoff[7] that $\lvert z_{in} \rvert = 332$ or 343 ohm. Then, since $T = 10.1\times10^{3}\,^oK$ and $\Omega = 2.7\times10^{-3}$ sterad, the received temperatures can be computed as $T_a = 1.89\times10^{4}\,\sigma\delta$ and $2.74\times10^{4}\,\sigma\delta$ for the 7.3π and the 9.5π radian lengths, respectively. Their ratio of 0.69 agrees fairly well with the observed ratio of 0.72. From these data, an average value of $\sigma\delta$ is computed, i.e., $\sigma\delta \approx 1.87\times10^{-4}$ mho.

4. Conclusions

An investigation has been made of the spatial distribution of the radiant energy emitted by a body for wavelengths at which the body dimensions and the wavelength are of the same order of magnitude. It is shown both theoretically and experimentally that in such cases the radiation pattern has the following characteristics:

1. It exhibits pronounced minima and maxima.
2. It is sensitive to the radian dimensions of the body.
3. It can have a well-defined polarization.
4. It is not, in general, a maximum in the direction for which the radiator subtends the maximum solid angle.

Although it has been widely assumed that interference effects are not observable using a spatially extended incoherent source, the experiments reported in this paper provide a successful demonstration of an interference phenomenon using such a source.

Finally, it is worthwhile to recall that simply by invoking the thermodynamic principle of the detailed balancing of radiation one can compute the spectral absorptivity of a body from its spectral thermal radiation pattern or vice versa. Thus, it follows that the spectral absorptivity of a body also exhibits the above-itemized characteristics at wavelengths which are of the order of the body dimensions.

5. Acknowledgement

The author wishes to acknowledge the many helpful discussions with C. H. Papas throughout the course of this work. Valuable consultation was also given by G. J. Stanley on radiometer principles and practices during the design of the equipment for the experiments.

The author wishes to express his appreciation to G. F. Smith who encouraged this work. This research was supported in part by a fellowship grant from the Hughes Aircraft Company.

References

1. H. Nyquist, "Thermal Agitation of Electric Charge in Conductors" Phys. Rev. 32, 110-113 (1928).

2. P. Parzen and L. Goldstein, "Current Fluctuations in D.C. Gas Discharge Plasma", Phys. Rev. 79, 190 (1950).

3. J. B. Johnson, "Thermal Agitation of Electricity in Conductors", Phys. Rev. 32, 97-109 (1928).

4. W. W. Mumford, "A Broad-Band Microwave Noise Source", Bell System Tech. J. 28, 608-618 (1949).

5. M. A. Leontovich and S. M. Rytov, Zhur. Exp. Teor. Fiz. 23, 246 (1952).

6. H. G. Booker, "Slot Aerials and Their Relation to Complementary Wire Aerials", J. Inst. Elec. Engrs (London) 93, Part IIIA, No.4 (1946).

7. S. A. Schelkunoff and H. T. Friis, Antennas, Theory and Practice (John Wiley and Sons, Inc., New York, 1952), pp.553-556, p.418.

8. J. Weber, "Scattering of Electromagnetic Waves by Wires and Plates", Proc. Inst. Radio Engrs. 43, 82-89 (1955).

9. W. R. Smythe, Static and Dynamic Electricity (McGraw-Hill Book Company, Inc., New York, 1950), second edition, p. 496.

10. M. L. Levin and S. M. Rytov, "Thermal Radiation from a Thin Rectilinear Antenna", J. Tech. Phys. (U.S.S.R.) 25, No. 2, 323-332 (1955).

11. N. George, "Spatial Distribution of Thermal Radiation at Microwave Frequencies", Calif. Inst. of Tech., Antenna Lab. Report No. 18 (1959).

12. V. Westberg, "Measurements of Noise Radiation at 10 cm from Glow Lamps", Chalmers Tekn. Hogsk. Handl., No. 180 (1956).

13. A. von Engel, Ionized Gases (Oxford Univ. Press, London 1955), p. 215.

14. S. Silver, Microwave Antenna Theory and Design (McGraw-Hill Book Company, Inc., New York, 1949), pp. 574-578.

15. R. H. Dicke, "The Measurement of Thermal Radiation at Microwave Frequencies", Rev. Sci. Instr. 17, 268-275 (1946).

DISTRIBUTION OF REPORTS

AF18(600)-1113

Commander, ATTN: SRY
AF Office of Scientific Res. 3
Washington 25, D. C.

Commander, ATTN: SRLT
AF Office of Scientific Res. 2
Washington 25, D. C.

Commander, ATTN: WCOSI
Wright Air Development Center 4
Wright-Patterson A.F. Base
Ohio

Commander, ATTN: CROT
AF Cambridge Research Center 1
L.G. Hanscom Field
Bedford, Massachusetts

Commander, ATTN: RCSSLD
Rome Air Development Center 1
Griffiss A.F. Base
Rome, New York

Commander, European Office 2
Air Research and Dev. Command
The Shell Building
47 rue Cantersteen
Brussels, Belgium

P.O. Box AA 1
Wright-Patterson A.F. Base
Ohio

Armed Services Tech.Inf.Agency 10
ATTN: TIPDR
Arlington Hall Station
Arlington 12, Virginia

Director of Res. and Dev. 1
Headquarters, USAF
ATTN: AFDRD
Washington 25, D. C.

Office of Naval Research 1
Department of the Navy
ATTN: Code 420
Washington 25, D. C.

Director, Naval Research Lab. 1
ATTN: Technical Inf. Officer
Washington 25, D. C.

Director, Army Research Office 1
Research and Development
Department of the Army
Washington 25, D. C.

Chief, Physics Branch 1
Division of Research
U.S. Atomic Energy Commission
Washington 25, D. C.

U.S. Atomic Energy Commission 1
Tech. Information Extension
P.O. Box 62
Oak Ridge, Tennessee

Natl. Bureau of Standards 1
Library, Room 203, NW Bldg.
Washington 25, D. C.

Physics Program 1
National Science Foundation
Washington 25, D. C.

Director, Office of Ordnance Res. 1
Box CM, Duke Station
Durham, North Carolina

Director, Dept. of Commerce 1
Office of Technical Services
Washington 25, D. C.

ARO, Inc. 1
ATTN: AEOI
Tullahoma, Tennessee

Commander, Air Proving Ground 1
ATTN: ACOT
Eglin A.F. Base, Florida

Commander 1
A.F. Flight Test Center
ATTN: FTOTL
Edwards A.F. Base, California

Commander 1
ATTN: ORDXR-OTL
Army Rocket and Guided Missile Ag.
Redstone Arsenal, Alabama

Commander 1
AF Special Weapons Center
ATTN: SWOI
Kirtland A.F. Base, New Mexico

Commander 1
AF Missile Development Center
ATTN: HDOI
Holloman A.F. Base, New Mexico

Commandant, ATTN: MCLI 1
A.F. Institute of Technology
Wright-Patterson A.F.Base, Ohio

Commander, ATTN: WDSOT 1
AF Ballistic Missile Division
AF Unit Post Office
Los Angeles 45, California

Commander 4
Air Res. and Dev. Command
Andrews AF Base,
Washington 25, D. C.
ATTN: RDR 1 copy
RDRR 1 copy
RDSFI-1 2 cc

Commanding General 1
U.S. Army Signal Corps
Research and Development Lab.
ATTN: SIGFM/EL-RPO
Ft. Monmouth, New Jersey

National Aeronautics and Space Administration 6
Washington 25, D. C.

Advanced Research Projects Ag. 1
Washington 25, D. C.

Rand Corporation 1
1701 Main Street
Santa Monica, California

Director, AUL 9663 1
Air University Library
Maxwell A.F. Base, Alabama

Chairman (DRB/DSIS) 1
Canadian Joint Staff
2450 Massachusetts Ave, NW
Washington 25, D. C.

Applied Mechanics Review 1
Southwest Research Institute
8500 Culebra Road
San Antonio 6, Texas

Inst. of the Aeronautical Sc. 1
2 East 64th Street
New York 16, New York
ATTN: Librarian

Exchange and Gift Division 1
Library of Congress
Washington 25, D. C.

Remington Rand Univac 1
Div. of Sperry Rand Corp.
19th St. and W.Allegheny Ave.
Philadelphia 29, Pennsylvania

Director, 1
Res. Lab. for Electronics
Massachusetts Inst. of Tech.
Cambridge 39, Massachusetts

Dean F. E. Terman 1
Electronics Research Laboratory
Stanford University
Stanford, California

Professor E. Weber 1
Microwave Research Laboratory
Polytechnic Inst.of Brooklyn
Brooklyn, New York

Head 1
G.E. Microwave Laboratory
601 California Avenue
Palo Alto, California

Professor T. E. Tice 1
Dept. of Electrical Engineering
Ohio State University
Columbus 10, Ohio

Dr. R. W. P. King 1
Harvard University
Cambridge, Massachusetts

General Electric Company 1
Missile and Ordnance Systems
3198 Chestnut Street
Philadelphia 4, Pennsylvania
ATTN: Library Manager

Professor John Hoffman 1
Dept. of Electrical Engineering
University of Illinois
Champaign, Illinois

Professor W. G. Shepherd 1
Dept. of Electrical Engineering
University of Minnesota
Minneapolis, Minnesota

Technical Library 1
Research and Dev. Labs.
Hughes Aircraft Company
Culver City, California

Dr. R. E. Hutter, Chief Eng. 1
Sylvania Elec. Products Inc.
P. O. Box 997
Mountain View, California

Professor P. Kusch 1
Radiation Laboratory
Columbia University
New York, New York

Dr. Donald E. Kerr 1
John Hopkins University
Department of Physics
Baltimore 18, Maryland

Dr. D. W. Healy
Electrical Engineering Dept. 1
Syracuse University Res. Inst.
Syracuse 10, New York

U. of Southern California 1
Electrical Engineering Dept.
Los Angeles 7, California
Attn: Z. Kaprielian

Stanford University 1
Microwave Research Laboratory
Stanford, California
Attn: M. Chodorow

University of Minnesota 1
Electrical Engineering Dept.
Minneapolis 14, Minnesota
Attn: H. Oskam

Northeastern University 1
Physics Department
Boston, Massachusetts
Attn: G. Lanza

University of New Hampshire 1
Department of Physics
Durham, New Hampshire
Attn: L. Mower

Rutgers University 1
Microwave Laboratory
New Brunswick, New Jersey
Attn: M. Sirkis

New York University 1
Inst. of Mathematical Sciences
25 Waverly Place
New York 3, New York
Attn: M. Kline

Oxford University 1
Oxford, England
Attn: H. Motz

University of Illinois 1
Dept. of Electrical Engineering
Urbana, Illinois
Attn: P. Coleman

Stevens Inst. of Technology 1
Physics Department
Hoboken, New Jersey
Attn: W. Bostick

University of California 1
Electronics Research Laboratory
Berkeley 4, California
Attn: J. Whinnery

Office of Naval Research 1
346 Broadway
New York 12, New York
Attn: I. Rowe

National Aeronautics and Space
Administration 1
1520 H Street, N.W.
Washington 25, D. C.
Attn: B. Mulcahy

Brooklyn Polytechnic Institute 1
Microwave Research Institute
55 Johnson Street
Brooklyn 1, New York
Attn: N. Marcuvitz

Dr. Glenn H. Keitel 1
Advanced Programs Section
Philco Corporation
3875 Fabian Way
Palo Alto, California